Inorg. Chem. **2004**, *43*, 2299–2307

On the Nature of the Lowest Triplet Excited State of the $[Rh_2(1,3\text{-diisocyanopropane})_4]^{2+}$ Ion

Irina V. Novozhilova, Anatoliy V. Volkov, and P. Coppens*

Department of Chemistry, State University of New York at Buffalo, Buffalo, New York 14260-3000

Received October 27, 2003

The nature of the ground state and the lowest triplet excited state of the $[Rh_2(1,3\text{-diisocyanopropane})_4]^{2+}$ ion have been investigated by the density functional theory. Two locally stable geometrical conformations are found on the potential energy surfaces of both the ground and excited states, corresponding to the eclipsed and twisted conformations, the eclipsed conformation being more stable and having the shorter Rh–Rh bond length. While the Rh–Rh distances of the two conformations differ by ∼0.4 Å, they shorten to the same value upon excitation (∼3.1 Å). The excited state originates from the d_{z^2}* (metal antibonding) to p_z (ligand–metal bonding) electronic transition. The Mayer Rh–Rh bond order increases from ∼0.2 to more than 0.8 upon excitation, while the Rh–C_N bond order shows a slight decrease. A topological bond path between the Rh atoms is found in both the ground and excited states, while the electron localization function (ELF) indicates weak Rh–Rh covalent bonding for the excited state only.

Introduction

As part of our program of excited-state structure determination by time-resolved photocrystallography,[1] we are performing theoretical calculations on isolated complexes to gain insight into the effect of the crystal matrix on geometry changes occurring during photoexcitation. We report here on a member of a series of d^8-d^8 binuclear complexes that show significant metal−metal bond shortening on excitation.

$[Rh_2(I)(bridge)_4]^{2+}$, bridge = 1,3-diisocyanopropane (further in the text abbreviated as $[Rh_2(diprop)_4]^{2+}$), has a paddle-wheel structure. The $[Rh_2(diprop)_4]^{2+}$ complex was first synthesized in 1976 by Gray et al.,[2] who also reported on its excited-state reactivity.[3] The 546-nm irradiation of $[Rh_2(diprop)_4]^{2+}$ in aqueous solutions of hydrohalic acids (HX) results in production of H_2 and formation of a d^7-d^7 $[Rh_2(diprop)_4X_2]^{2+}$ species. Since such binuclear complexes have relatively long phosphorescence lifetimes, they were among the first to be considered as candidates for solar energy conversion devices.[3−5]

Spectroscopic Properties

The polarized UV−vis absorption spectrum of a single crystal of the BPh_4^- salt at 5 K exhibits a strong band at 565 nm attributable to a fully allowed $^1A_1 \rightarrow {}^1A_2$ excitation (D_4 point group designations). The spectrum also shows a vibronically structured band ($\lambda_{max} \sim 670$ nm), assigned to the $^1A_1 \rightarrow E$ ($^3A_2$) transition, consisting of a very long progression with a separation of 143 cm^{-1}.[6] In time-resolved resonance Raman studies of the ground and excited states, this excited-state frequency was assigned to the $\nu(Rh_2)$ stretching, increased from the ground-state value of 85 cm^{-1}.[7] From the Franck−Condon analysis of the vibrational fine-structure of the 670-nm band, a Rh−Rh shortening on excitation of 0.31 Å was derived, corresponding to an excited-state Rh−Rh distance of 2.93 Å, using the ground-state Rh−Rh distance of 3.242(1) Å from a room-temperature

* To whom correspondence should be addressed. E-mail: coppens@acsu.buffalo.edu.

(1) (a) Coppens, P.; Novozhilova, I. V. *Faraday Discuss.* **2002**, *122*, 1−11. (b) Coppens, P. *Chem. Commun.* **2003**, 1317−1320.
(2) Lewis, N. S.; Mann, K. R.; Gordon, J. G., II; Gray, H. B. *J. Am. Chem. Soc.* **1976**, *98*, 7461−7463.
(3) Mann, K. R.; Lewis, N. S.; Miskowski, V. M.; Erwin, D. K.; Hammond, G. S.; Gray, H. B. *J. Am. Chem. Soc.* **1977**, *99*, 5525−5526.
(4) (a) Miskowski, V. M.; Sigal, I. S.; Mann, K. R.; Gray, H. B. *J. Am. Chem. Soc.* **1979**, *101*, 4383−4385. (b) Mann, K. R.; Bell, R. A.; Gray, H. B. *Inorg. Chem.* **1979**, *18*, 2671−2673. (c) Sigal, I. S.; Mann, K. R.; Gray, H. B. *J. Am. Chem. Soc.* **1980**, *102*, 7252−7256. (d) Gray, H. B.; Maverick, A. W. *Science* **1981**, *214*, 1201−1205.
(5) Harvey, P. D. *Coord. Chem. Rev.* **2001**, *219*−*221*, 17−52 and references therein.
(6) (a) Rice, S. F.; Gray, H. B. *J. Am. Chem. Soc.* **1981**, *103*, 1593−1595. (b) Rice, S. F.; Miskowski, V. M.; Gray, H. B. *Inorg. Chem.* **1988**, *27*, 4704−4708.
(7) (a) Dallinger, R. F.; Miskowski, V. M.; Gray, H. B.; Woodruff, W. H. *J. Am. Chem. Soc.* **1981**, *103*, 1595−1596. (b) Doorn, S. K.; Gordon, K. C.; Dyer, R. B.; Woodruff, W. H. *Inorg. Chem.* **1992**, *31*, 2284−2285.

10.1021/ic035243h CCC: $27.50
Published on Web 03/09/2004

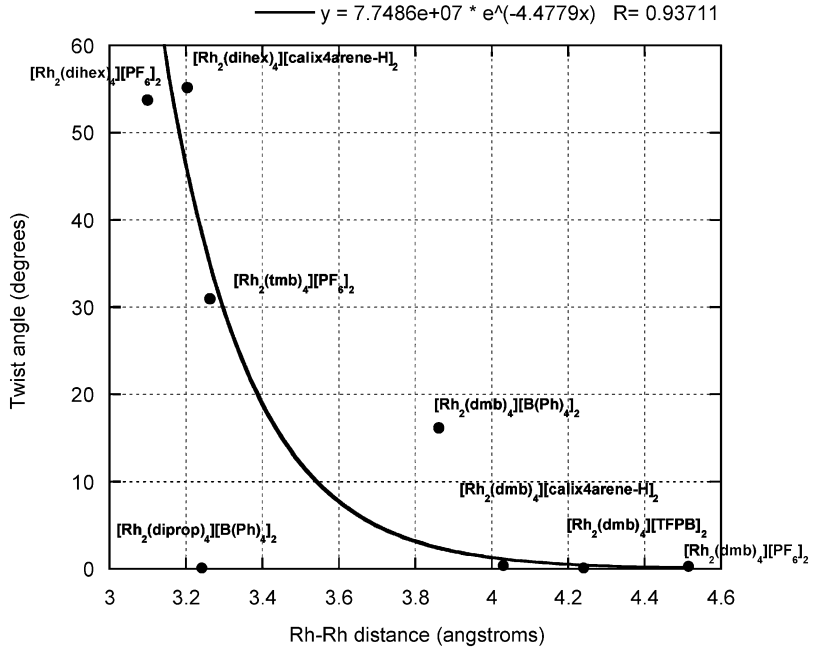

Figure 1. Rh−Rh distance vs C−Rh−Rh−C dihedral (twist) angle in various $[Rh_2(diiso)_4][Y]_2$ complexes. Abbreviations: diprop, 1,4-diisocyanopropane; tmb, 2,5-diisocyano-2′,5′-dimethylhexane; dmb (dimen), 1,8-diisocyano-*p*-menthane; dihex, 1,6-diisocyanohexane; TFPB, tetrakis[3,5-bis(trifluoromethyl)-[phenyl]borate); BPh_4, $B(C_6H_5)_4$. $[Rh_2(diprop)_4][BPh_4]_2$, refs 8, 9; $[Rh_2(tmb)_4][PF_6]_2$, ref 8; $[Rh_2(dmb)_4][PF_6]_2$, $[Rh_2(dihex)_4][PF_6]_2$, $[Rh_2(dihex)_4][calix4arene-H]_2$, $[Rh_2(dmb)_4][calix4arene-H]_2$, ref 9; $[Rh_2(dmb)_4][B(Ph)_4]_2$, $[Rh_2(dmb)_4][TFPB]_2$, ref 14 and references therein.

crystal structure determination of $[Rh_2(diprop)_4](BPh_4)_2 \cdot CH_3CN$.[8] The latter value agrees reasonably well with our more recent low-temperature value of 3.2222(5) Å.[9] From time-resolved IR and Raman spectroscopic measurements of the ground and excited states of $[Rh_2(diprop)_4]^{2+}$, a small shortening of the Rh—C_N bond (−0.022 Å) was deduced, while for the C≡N bond a very small change (+0.002 Å) was obtained.[7] The shortening of the Rh—Rh bond has been attributed to the promotion of an electron from an antibonding dσ* orbital to a weakly bonding pσ orbital, similar to the shortening that occurs on excitation of the d^8—d^8 $[Pt_2(pop)_4]^{4-}$ ion (pop = pyrophosphate, $(H_2P_2O_5)^{2-}$).[10]

Measurements of fluorescence and phosphorescence spectra of $[Rh_2(diprop)_4]^{2+}$ in acetonitrile solution at room temperature (294 K) gave a fluorescence lifetime $\tau_F < 2$ ns ($\lambda_{max} = 656$ nm) and a phosphorescence lifetime $\tau_P = 8.5$ (±5) μs ($\lambda_{max} = 800$ nm). The longer-lifetime emission has been assigned to the $^3A_2$ state.[11] The phosphorescence lifetime is temperature dependent, with the value of τ_P at 77 K reported as 16 μs, compared with the phosphorescence lifetimes of 25 ns at 300 K versus 20 μs at 77 K for $[Rh_2(tmb)_4]^{2+}$ (tmb = 2,5-diisocyano-2′,5′-dimethylhexane).[11−13]

Since the early work of Gray et al.,[2−4,6−8] a series of additional structural and spectroscopic studies on $[M_2(bridge)_4]^{2+}$ bridged binuclear complexes with M = Rh, Ir, where "bridge" is 1,8-diisocyano-*p*-menthane (dmb or dimen), 1,4-diisocyanobutane, or tmb, have been reported.[5] X-ray crystal structures of dimen-bridged diisocyano M(I) complexes summarized by Exstrom et al.[14] indicate the M−M distances decrease with increasing dihedral twist angle C−M-M−C with values ranging from 4.6 to 3.2 Å and from 0° to 31°, respectively. A survey including all currently reported binuclear Rh structures extends the angular range to 56° (Figure 1) and confirms this to be a general trend. The structure of $[Rh_2(dmb)_4][B(Ph)_4]_2$ lies off the curve and may have to be re-examined. The conformational diversity of $[M_2(bridge)_4]^{2+}$ complexes has been referred to as deformational isomerism.[14]

Computational Details

Calculations were carried out with the ADF2002 suite of programs. The local density functional of Vosko, Wilk, and Nusair (VWN)[15] was employed. The gradient correction was introduced with the exchange functional of Perdew and Wang (PW86)[16] and the correlation functional of Lee, Yang, and Parr (LYP).[17] The atomic orbitals of rhodium were described by a triple-ζ Slater-type basis set (ADF database TZP, formerly IV). For the carbon,

(8) Mann, K. R.; Thich, J. A.; Bell, R. A.; Coyle, C. L.; Gray, H. B. *Inorg. Chem.* **1980**, *19*, 2462−2468.
(9) Gerlits, O.; Coppens, P. To be published.
(10) Novozhilova, I. V.; Volkov, A. V.; Coppens, P. *J. Am. Chem. Soc.* **2003**, *125*, 1079−1087.
(11) (a) Miskowski, V. M.; Nobinger, G. L.; Kliger, D. S.; Hammond, G. S.; Lewis, N. S.; Mann, K. R.; Gray, H. B. *J. Am. Chem. Soc.* **1978**, *100*, 485−488. (b) Milder, S. J.; Goldbeck, R. A.; Kliger, D. S.; Gray, H. B. *J. Am. Chem. Soc.* **1980**, *102*, 6761−6764.
(12) Rice, S. F.; Milder, S. J.; Gray, H. B.; Goldbeck, R. A.; Kliger, D. S. *Coord. Chem. Rev.* **1982**, *43*, 349−354.
(13) Smith, D. C.; Miskowski, V. M.; Mason, W. R.; Gray, H. B. *J. Am. Chem. Soc.* **1990**, *112*, 3759−3767.
(14) Exstrom, C. L.; Britton, D.; Mann, K. R.; Hill, M. G.; Miskowski, V. M.; Schaefer, W. P.; Gray H. B.; Lamanna, W. M. *Inorg. Chem.* **1996**, *35*, 549−550.
(15) Vosko, S. H.; Wilk, L.; Nusair, M. *Can. J. Phys.* **1980**, *58*, 1200−1211.
(16) Perdew, J. P.; Wang, Y. *Phys. Rev. B* **1986**, *33*, 8800−8802.
(17) Lee, C.; Yang, W.; Parr, R. G. *Phys. Rev. B* **1988**, *37*, 785−789.

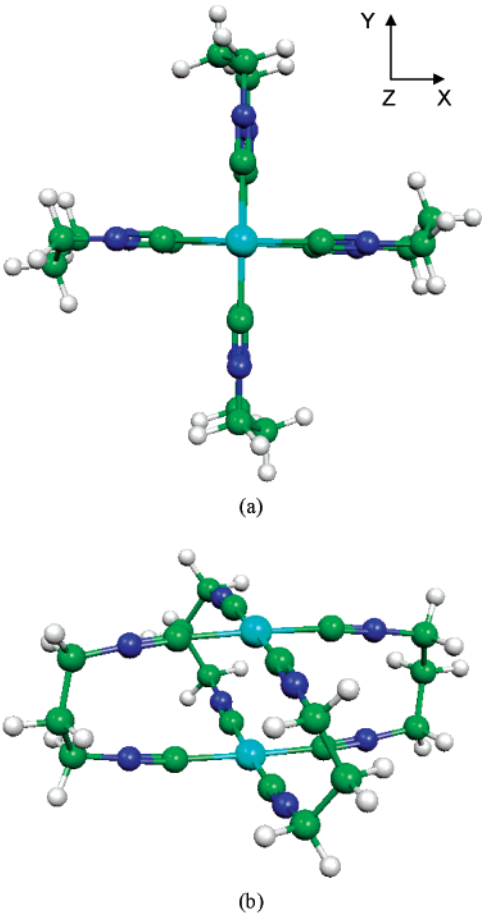

Figure 2. 3D view of the eclipsed geometry corresponding to the global minimum on the ground-state PES of the $[Rh_2(diprop)_4]^{2+}$ looking down the *z*-axis (a) and along the *z*-axis (b).

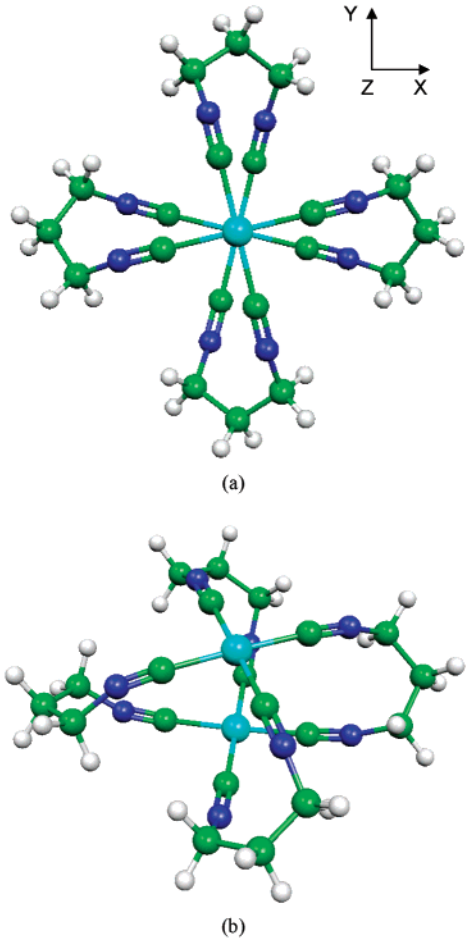

Figure 3. 3D view of the twisted geometry corresponding to the local minimum on the ground-state PES of the $[Rh_2(diprop)_4]^{2+}$ looking down the *z*-axis (a) and along the *z*-axis (b).

nitrogen, and hydrogen atoms double-ζ Slater-type basis sets with one polarization function added (ADF database DZP, formerly III) were used. The (1s2s2p3s3p3d)[28] core shell of Rh and the (1s)^2 core shells of C and N were treated in the frozen core (FC) approximation. Scalar relativistic effects were taken into account with the zeroth order regular approximation (ZORA).[18] The integrals were evaluated numerically with an accuracy of 8 significant digits. A set of auxiliary s, p, d, f, and g functions, centered on all nuclei, was used to fit the electron density, together with both Coulomb and exchange potentials in each SCF cycle. Geometry conversion was considered complete when the Cartesian gradients fell below the threshold of 10^{-4} Hartree/Å (compared to a 10^{-2} default value). All optimized molecular geometries were confirmed as true energy minima by the positive eigenvalues in the Hessian matrices, from which IR frequencies were calculated. Time-dependent density functional theory (TD-DFT)[19] calculations of vertical excitation energies were carried out with the same functionals and basis sets used in the geometry optimization. The Davidson algorithm was used, in which the error tolerances in the square of the excitation energies and trial-vector orthonormality criterion were set to 10^{-8} and 10^{-10}, respectively. The molecular orbitals were visualized with MOLDEN3.7.[20] The ADF output was converted to MOLDEN format using ADF2MOLDEN program.[21] Deformation density maps were calculated with the ADF auxiliary program DENSF and converted to GNUPLOT format by the ADF auxiliary program CNTRS. The electron localization function (ELF) was calculated using the program written by J. Autschbach and T. Ziegler[22] and implemented in the ADF auxiliary program DENSF. ELF and spin-density 3D-representations were prepared in MOLEKEL4.1.[23] Mayer bond orders were calculated with the program MAYER.[24]

(18) (a) Chang, C.; Pelissier, M.; Durand, M. *Phys. Scr*. **1986**, *34*, 394−404. (b) van Lenthe, E.; Baerends, E. J.; Snijders, J. G. *J. Chem. Phys*. **1993**, *99*, 4597−4610. (c) van Lenthe, E.; Baerends, E. J.; Snijders, J. G. *J. Chem. Phys*. **1994**, *101*, 9783−9792. (d) van Lenthe, E.; van Leeuwen, R.; Baerends, E. J.; Snijders, J. G. *Int. J. Quantum Chem*. **1996**, *57*, 281−293.
(19) (a) van Gisbergen, S. J. A.; Kootstra, F.; Schipper, P. R. T.; Gritsenko, O. V.; Snijders, J. G.; Baerends, E. J. *Phys. Rev. A* **1998**, *57*, 2556−2571. (b) Jamorski, C.; Casida, M. E.; Salahub, D. R. *J. Chem. Phys*. **1996**, *104*, 5134−5147. (c) Bauernschmitt, R.; Ahlrichs, R. *Chem. Phys. Lett*. **1996**, *256*, 454−464.
(20) Schaftenaar, G.; Noordik, J. H. *J. Comput.-Aided Mol. Des*. **2000**, *14*, 123−134.
(21) Volkov, A. V. *ADF2MOLDEN*; State University of New York at Buffalo: Buffalo, NY, 1999.
(22) Autschbach, J.; Ziegler, T. The University of Calgary: Calgary, Canada, 2000.
(23) Flükiger, P.; Lüthi, H. P.; Portmann, S.; Weber, J. *MOLEKEL-4.1*; Swiss Center for Scientific Computing: Manno, Switzerland, 2000−2001.
(24) Bridgeman, A. J.; Empson, C. J. *MAYER*; The University of Hull: Hull, U.K., 2003. Freely available on the worldwide web from http://www.hull.ac.uk/php/chsajb/mayer/. Bridgeman, A. J.; Cavigliasso, G.; Ireland, L. R.; Rothery, J. *J. Chem. Soc., Dalton Trans*. **2001**, 2095−2108.
(25) Hirshfeld, F. L. *Theor. Chim. Acta* **1977**, *44*, 129−138.
(26) Bader, R. W. F. *Atoms in Molecules: a Quantum Theory*; Oxford University Press: Oxford, U.K., 1990.
(27) Mayer, I. *Chem. Phys. Lett*. **1983**, *97*, 270−274.
(28) Ortiz Alba, J. C.; Bo, C. *XAIM-1.0*; Universitat Rovira I Virgili: Tarragona, Spain; http://www.quimica.urv.es/XAIM, 1998.

Table 1. Selected Theoretical Bond Lengths (in Å) and Angles (in deg) of the Ground State in Comparison with the Experimental Structure, and Excited Triplet State of the $[Rh_2(diprop)_4]^{2+}$ Ion

	exptl $[Rh_2(diprop)_4](BPh_4)_2$		theoretical $[Rh_2(diprop)_4]^{2+}$			
	eclipsed geometry		ground state		excited triplet state	
	295 K[a]	90 K[b]	eclipsed	twisted	eclipsed	twisted
Rh−Rh	3.242(1)	3.2222(5)	3.441	3.853	3.056	3.098
$Rh-C_N$	1.959(4), 1.960(4), 1.976(4), 1.960(4)	1.957(3), 1.969(3), 1.977(3), 1.971(3)	1.985	1.983	1.989	1.989
C−N	1.128(5), 1.144(6), 1.147(5), 1.146(5)	1.147(4), 1.145(4), 1.140(3), 1.142(4)	1.160	1.162	1.162	1.165
$N-C_{H2}$	1.434(7), 1.455(7), 1.443(5), 1.452(6)	1.443(4), 1.457(4), 1.444(3), 1.456(4)	1.418	1.422	1.417	1.428
$C_{H2}-C_{H2}$	1.447(8)	1.507(4)	1.522	1.522	1.521	1.523
	1.357(9)	*1.345(9), 1.474(5)*				
	1.515(5)	1.521(4)				
	1.402(10), 1.429(8)	*1.381(11), 1.481(4)*				
twist	0.0	0.0	2.3	26.8	1.4	28.0
E, H			−12.1607	−12.1238	−12.1063	−12.0657

[a] Reference 8. [b] Reference 9. Bonds in italic type correspond to disordered atomic positions.

Scheme 1

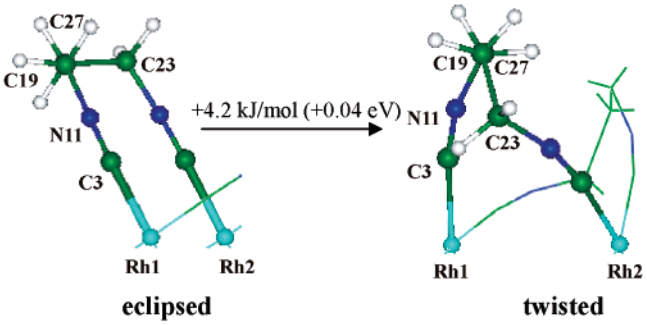

Results and Discussion

Ground-State Geometry. The ground-state potential energy surface (PES) of the $[Rh_2(diprop)_4]^{2+}$ ion shows two minima corresponding, respectively, to nearly eclipsed (C_4 symmetry) (Figure 2) and twisted (D_4 symmetry) (Figure 3) conformations, the former being more stable by ∼1.0 eV (because the C_4 point group is not yet supported in ADF, the lower symmetry (C_2) was used to optimize the eclipsed geometry). Selected geometrical parameters for both states are given in Table 1. The calculated Rh−Rh distance in the eclipsed structure is equal to 3.44 Å with a $C_N-Rh-Rh-C_N$ twist angle of only ∼2°, but it is longer by ∼0.4 Å in the twisted conformation which has a twist angle of ∼27°. This difference is opposite to the trend observed in published crystal structures, in which the larger twist angles correspond to shorter Rh−Rh distances (Figure 1). The difference may be related to the short length of the propane bridge, which necessitates a distortion of the ligand on twisting. This is confirmed by the theoretically optimized geometries, which show a reduction of the N11−C19−C27−C23 torsion angle from 68.0° to 41.9° and a decrease in the C3−N11−C19 angle from 177.6° to 164.2°. The energy change due to internal rotation around the C19−C27 bond of the ligand is calculated to be 4.2 kJ/mol (Scheme 1).

The eclipsed conformation of $[Rh_2(diprop)_4]^{2+}$ from theory agrees reasonably well with that of the $[Rh_2(diprop)_4]^{2+}$ ion in crystals of $[Rh_2(diprop)_4](BPh_4)_2 \cdot CH_3CN$ (Table 1), though the calculated Rh−Rh distance is 0.2 Å longer than the observed value. The Rh−Rh potential is obviously very shallow as evidenced by the value of the stretching frequency, which is only 71 cm^{-1} according to the calculation and 79 cm^{-1} according to the experiment (Table 3). With the corresponding harmonic force constant, a lengthening of the Rh−Rh distance to 4.2 Å would only require 0.010 H, or 0.27 eV, a value considerably less than the calculated energy difference between the eclipsed and twisted conformations of the $[Rh_2(diprop)_4]^{+}$ ion.

Attempts to optimize the twisted structure with Rh−Rh distances shorter than those in the eclipsed conformation were unsuccessful as the structure invariably returned to the geometry with the longer Rh−Rh distance.

There are no significant differences in other bond lengths or angles between the eclipsed and twisted conformations.

Excited-State Geometry. Selected structural parameters, as obtained by the optimization of the lowest-energy triplet excited state, are presented in Table 1. As in the ground state, both eclipsed (E_{tr}^{eclip}) and twisted (E_{tr}^{twist}) conformations are found to correspond to minima on the excited-state potential energy surface, the eclipsed conformation, ES_{tr}^{eclip}, being more stable by 0.041 H, compared with 0.037 H for the ground state, GS^{eclip}. However, in contrast to the ground state, in the excited state the Rh−Rh distances of the two conformations differ by only 0.04 Å.

Table 2. Magnitude of the Rh−Rh and $Rh-C_N$ Bond (in Å) Changes upon Singlet−Triplet Excitation in the $[Rh_2(diprop)_4]^{2+}$

		Theory	
	expt	eclipsed	twisted
Rh−Rh	−0.31[a]	−0.385	−0.755
$Rh-C_N$	−0.022[b]	+0.004	+0.006

[a] Reference 6b. Franck−Condon value from polarized single-crystal absorption spectroscopy at 5 K, $[Rb_2(diprop)_4](BPh_4)_2 \cdot CH_3CN$. [b] Reference 7. Empirical result from time-resolved resonance Raman spectrum in CH_3CN solution.

Table 3. Selected Vibrational Modes of $[Rh_2(diprop)_4]^{2+}$

			theory			
mode, cm^{-1}	expt, eclipsed		eclipsed		twisted	
	ground	excited	GS^{eclip}	ES_{tr}^{eclip}	GS^{twist}	ES_{tr}^{twist}
$\nu(Rh_2)$	79[a]	144[a]	71	117	44	111
	85[b]	149[b]				
$\nu(C\equiv N)$[c]	2193[d]	2177[d]	2291	2219	2276	2193
		∼2150[b]				

[a] Reference 7a, CH_3CN solution. [b] Reference 6b, $[Rb_2(diprop)_4](BPh_4)_2 \cdot CH_3CN$ crystal. [c] There are a total of eight C≡N vibrational modes. [d] Reference 7b, CH_3CN solution.

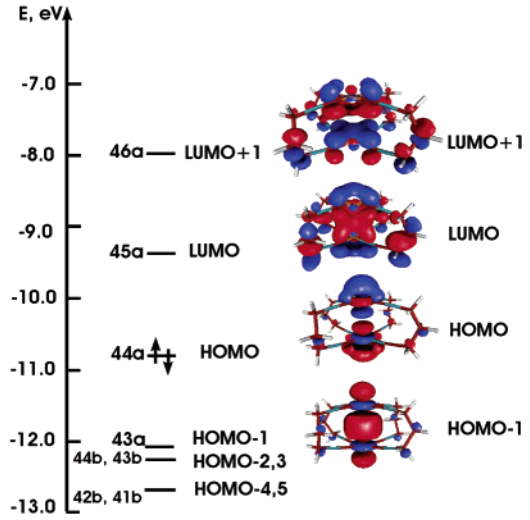

Figure 4. Ordering of the frontier molecular orbitals of the eclipsed ground state. Plotted isosurface value is 0.03 au for LUMO and LUMO+1, and 0.02 au for HOMO and HOMO−1. C_2 designations are used to identify the orbitals.

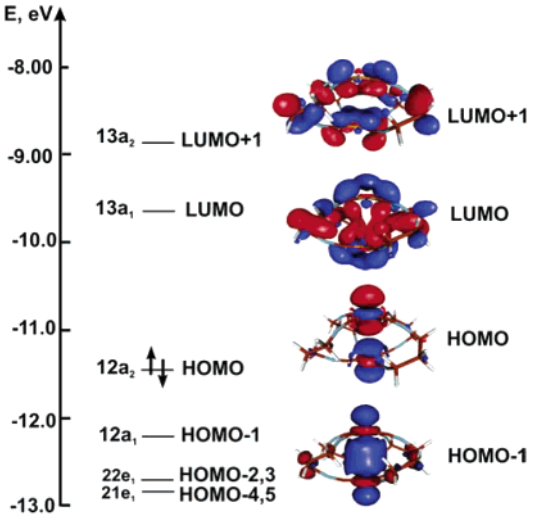

Figure 5. Ordering of the frontier molecular orbitals of the twisted geometry on the ground-state PES. Plotted isosurface value is 0.03 au for LUMO and LUMO+1, and 0.02 au for HOMO and HOMO−1. D_4 designations are used to identify the orbitals.

The calculations predict a Rh−Rh shortening for the eclipsed structure of 0.39 Å in reasonable agreement with the Franck−Condon value of 0.31 Å[6] discussed earlier. For the twisted conformation, a Rh−Rh shortening of 0.76 Å is obtained (Table 2), leading to almost equal excited-state Rh−Rh distances for the two conformations. The shortening of the Rh−Rh bond in the excited state is also reflected in the calculated stretching frequency ν(Rh$_2$) which increases upon excitation in agreement with experimental results (Table 3).

Our calculations predict a small increase of the Rh−C$_N$ bond in the excited state. This contrasts with the conclusion derived from the time-resolved resonance Raman measurements in CH$_3$CN solution[7a] (Table 2) based on the assignment of the 467 cm^{-1} ground-state frequency to the Rh−C$_N$ stretching mode. However, examination of the normal modes from the calculation indicates that this frequency cannot be assigned to a single bond as it involves displacements not only of Rh and C$_N$ but also of several other atoms of the ligand, a limitation mentioned in the spectroscopic derivation of the bond length change.[7b] There are in fact ten calculated vibrational modes in the 420−500 cm^{-1} region all involving displacements of Rh, C$_N$, and other ligand atoms, with some of the modes showing increasing and some decreasing frequencies upon excitation.

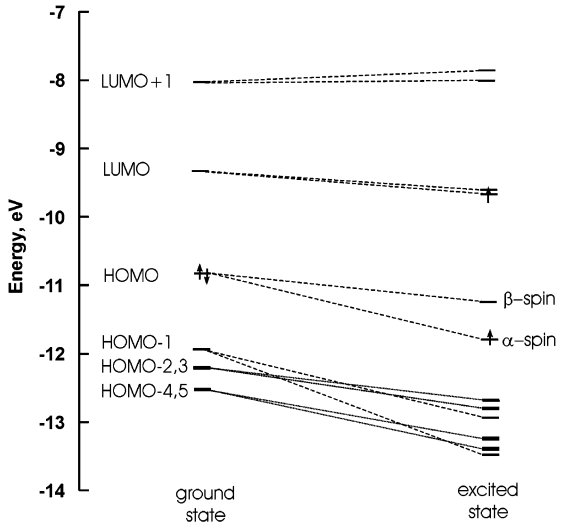

Figure 6. Energy levels of the molecular orbitals just above and below the HOMO−LUMO level in the eclipsed ground state and excited triplet state from the calculations. The arrows indicate the electron population of the highest occupied orbitals in each case.

Table 4. Hirshfeld and Bader Charge Analyses of the Eclipsed[a] and Twisted[b] Conformations on the Ground- and Excited-State PES of [Rh$_2$(diprop)$_4$]$^{2+}$

	q(GS)		q(ES$_{tr}$)		Δq(ES$_{tr}$−GS)	
atom	Hirshfeld	Bader	Hirshfeld	Bader	Hirshfeld	Bader
Rh	0.156	2.644	0.230	2.733	+0.074	+0.089
	0.182	2.666	0.256	2.752	+0.074	+0.086
C$_{Rh}$	0.02	0.73	0.01	0.70	−0.01	−0.03
	0.03	0.72	0.02	0.68	−0.01	−0.04
N	−0.04	−1.17	−0.04	−1.16	0.0	+0.01
	−0.04	−1.16	−0.04	−1.13	0.0	+0.03
N−**C**$_{H2}$−C$_{H2}$	0.02	0.39	0.02	0.39	0.0	0.0
	0.02	0.38	0.02	0.37	0.0	+0.01
C$_{H2}$−**C**$_{H2}$−C$_{H2}$	−0.05	0.01	−0.05	0.01	0.0	0.0
	−0.05	0.01	−0.05	0.01	0.0	0.0

[a] First line. [b] Second line.

Molecular Orbitals. Consistent with the interpretation of the experimental observations, the HOMO consists mainly of d_{z^2} atomic orbitals of the rhodium atoms and is antibonding in the metal−metal region (Figures 4 and 5). The LUMO, on the other hand, is bonding in the Rh−C$_N$ and Rh−Rh regions. According to the calculations (Table S1), the rhodium atomic orbital contribution to the LUMO amounts to only 18% (p_z Rh), while the ligand p_z atomic orbitals give a much larger contribution (44% for p_z C$_N$ and 24% for p_z N). This is manifested in the large overlapping regions with Rh atomic orbitals evident in Figures 4 and 5. The HOMO−1 orbital is a bonding metal−metal d_{z^2}−d_{z^2} orbital, which is paired with the antibonding d_{z^2}−d_{z^2} HOMO. The HOMO−2,3 and HOMO−4,5 are primarily d_{xz}, d_{yz} rhodium orbitals with some ligand contribution (Table S1).

The molecular orbitals in the ground and excited states are rather similar (Table S1). However, the occupied orbitals

Table 5. Difference in the Mulliken Population, $\Delta P(ES_{tr}-GS)$, of the Atomic Valence Orbitals for the Eclipsed Geometry of $[Rh_2(diprop)_4]^{2+}$[a]

ΔRh	s	p_x	p_y	p_z	d_{x^2}	d_{xy}	d_{xz}	d_{y^2}	d_{yz}	d_{z^2}
$n = 4$[b]	−0.002	0.005	0.005	0.022	−0.009	0.045	0.059	0.009	0.059	−0.284
$n = 5$[b]	−0.114	0.005	0.005	0.114						

atom[c]	2s	$2p_x$	$2p_y$	$2p_z$
ΔC3	−0.017	0.0	−0.004	0.043
ΔN11	0.002	−0.011	−0.002	0.014
ΔC19	−0.001	−0.004	−0.003	0.006
ΔC27	0.0	0.003	−0.003	0.0

[a] Similar values are obtained for the twisted geometry (Table S3). [b] n, the principal quantum number. [c] See Scheme 1 for atom numbering.

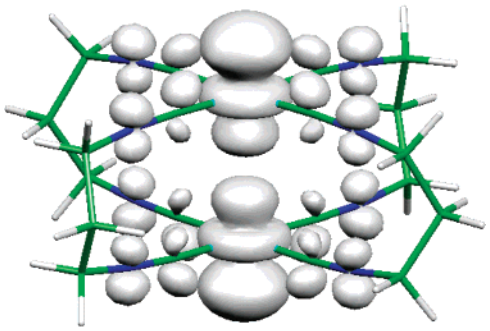

Figure 7. Representation of the spin density ("spin up" density minus "spin down" density) of the triplet $[Rh_2(diprop)_4]^{2+}$. Eclipsed geometry is shown. Twisted geometry gives similar picture. Plotted isosurface value 0.003 au.

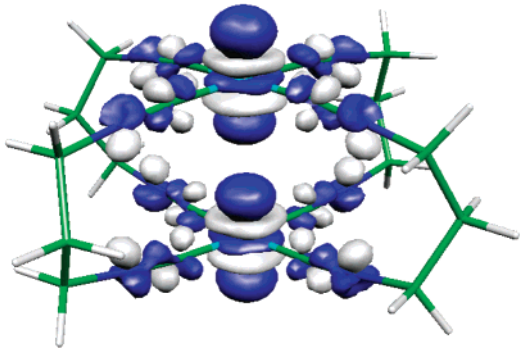

Figure 8. Excitation difference electron density of $[Rh_2(diprop)_4]^{2+}$. The eclipsed geometry is shown. The twisted geometry gives similar picture. Plotted isosurface value 0.003 au, gray lobes are positive (accumulation of density).

Table 6. Mayer Bond Orders for the Rh−Rh and Rh−C_N Bonds of $[Rh_2(diprop)_4]^{2+}$

	GS^{eclip}	ES_{tr}^{eclip}	GS^{twist}	ES_{tr}^{twist}
Rh−Rh	0.17	0.83	0.07	0.83
Rh−C_N	0.32	0.29	0.34	0.30

are generally lower in energy in the excited state (Figure 6). This is most pronounced for the HOMO−1 level of the ground state, which is stabilized by 1.6 eV in the excited state. The degenerate HOMO−2,3 and HOMO−4,5 levels (E orbitals if the D_4 symmetry notation is used) are split in the excited state (Figure 6) and also lower in energy than the corresponding ground-state orbitals.

Hirshfeld and Bader Charge Analyses. The values of the difference between the atomic charges in the ground and excited states, ($\Delta q(ES_{tr}-GS)$), for the Hirshfeld[25] and Bader[26] definitions agree remarkably well for all atoms, though, as is well-known, the two types of charges themselves differ widely. Comparison of the ground- and excited-state values (Table 4) reveals that upon excitation the rhodium atoms become more positive and the adjacent carbon atoms less positive. Changes in the charges of all other atoms are insignificant.

The Mulliken population analysis of the atomic orbitals (Table 5) shows a decrease in the population of the Rh d_{z^2} and 5s orbitals upon excitation, while the p_z orbitals of Rh, and the C and N atoms of the CN group, increase in population. The unpaired spin density is mainly localized on the rhodium atoms (Table S2), though some degree of spin delocalization over the CN groups is evident (Figure 7). The Rh−Rh bond order as defined by Mayer[27] (Table 6) increases from a very small value to close to 1 (0.83), while the Rh−C_N bond order decreases slightly, in agreement with the calculated bond length changes, and similar to the results obtained previously for the $[Pt_2(pop)_4]^{4-}$ ion.[10]

The excitation electron-density difference map defined as $\rho_{excited} - \rho_{ground}$, with $\rho_{excited}$ transferred to the ground-state geometry to eliminate the effect of atomic motion, is shown in Figure 8. As may be expected, the features are most pronounced in the Rh−CN regions.

Absorption Spectrum. The electronic transition energies of $[Rh_2(diprop)_4]^{2+}$ calculated with TD-DFT are presented in Table 7, in which D_4 symmetry notation is used to identify the transitions. The lowest-energy transition corresponds to the spin-forbidden singlet−triplet ($^3A_2$) excitation from the antibonding HOMO to the bonding LUMO. The calculated values of the excitation energy for this transition are 1.39 and 1.72 eV, for the eclipsed and twisted geometries, respectively, compared to the experimental (single crystal) value of 1.85 eV.[6] The strong singlet−singlet HOMO−LUMO ($^1A_2$) transition is calculated at 1.84 and 2.13 eV, respectively, for the eclipsed and twisted geometries. In the twisted geometry, this $^1A_2$ transition blue shifts compared with the eclipsed geometry, in agreement with the difference between experimental single-crystal values for twisted $[Rh_2(tmb)_4](PF_6)_2 \cdot 2CH_3CN$ and eclipsed $[Rh_2(diprop)_4](BPh_4)_2 \cdot CH_3CN$.[6,8]

Our TD-DFT calculations are in accord with the experimental assignment of the HOMO to LUMO+1 ($^1A_1$ and $^3A_1$) transitions as corresponding to d_{z^2}* (metal antibonding) → p_z* (ligand−metal antibonding) excitations.

Topological Analysis of the Charge Density. The results of the topological analysis of theoretical charge density of $[Rh_2(diprop)_4]^{2+}$, obtained with the program XAIM-1.0,[28] are presented in Table 8. In both the ground state and excited

Table 7. TD-DFT Electronic Transition Energies (in eV) for [Rh$_2$(diprop)$_4$]$^{2+a}$

Γ_{D4}	GS^{eclip} C_2	GS^{twist} D_4	one-electron excitation	MO character	% MO eclipsed	% MO twisted	exptl[b] eV	exptl[b] nm
$^1A_2$	1.84 (0.0912)	2.13 (0.0739)	$12a_2 \rightarrow 13a_1$	$d_{z^2}^* \rightarrow p_z$	99	99	2.19	565
$^1A_1$	2.77 (0.44×10^{-5})	2.80	$12a_1 \rightarrow 13a_1$	$d_{z^2} \rightarrow p_z$	91	75		415
			$12a_2 \rightarrow 13a_2$	$d_{z^2}^* \rightarrow p_z^*$	9	25		
$^1A_1$	2.93 (0.27×10^{-5})	2.61	$12a_2 \rightarrow 13a_2$	$d_{z^2}^* \rightarrow p_z^*$	90	75	2.99	
			$12a_1 \rightarrow 13a_1$	$d_{z^2} \rightarrow p_z$	9	24		
$^1A_2$	4.06 (0.0078)	3.43 (0.0012)	$12a_1 \rightarrow 13a_2$	$d_{z^2} \rightarrow p_z^*$	51	100		
$^3A_2$	1.39	1.72	$12a_2 \rightarrow 13a_1$	$d_{z^2}^* \rightarrow p_z$	100	100	1.85	670
$^3A_1$	2.51	2.45	$12a_1 \rightarrow 13a_1$	$d_{z^2} \rightarrow p_z$	99	84	2.18	568
			$12a_2 \rightarrow 13a_2$	$d_{z^2}^* \rightarrow p_z^*$		16		
$^3A_1$	2.72	2.54	$12a_2 \rightarrow 13a_2$	$d_{z^2}^* \rightarrow p_z^*$	99	84	2.48	500
			$12a_1 \rightarrow 13a_1$	$d_{z^2} \rightarrow p_z$		16		
$^3A_2$	3.83	3.27	$12a_1 \rightarrow 13a_2$	$d_{z^2} \rightarrow p_z^*$	100	100		

[a] Nonzero oscillator strengths in parentheses. Only the lowest d_{z^2}, $d_{z^2}^*/p_z$, p_z^* transitions are listed. [b] Reference 6b, [Rb$_2$(diprop)$_4$](BPh$_4$)$_2$·CH$_3$CN, polarized single-crystal absorption spectroscopy at 5 K.

Table 8. Topological Properties (in au) at the Rh−Rh and Rh−C_N BCPs (3, −1) of the Ground State[a] and the Triplet State[b] of the Eclipsed [Rh$_2$(diprop)$_4$]$^{2+c}$

(3, −1)	$\rho(\mathbf{r}_c)$	λ_1	λ_2	λ_3	$\nabla^2\rho_c$	ϵ	$H(\mathbf{r}_c)$	$H(\mathbf{r}_c)/\rho_c(\mathbf{r}_c)$	$G(\mathbf{r}_c)$	$G(\mathbf{r}_c)/\rho(\mathbf{r}_c)$	$V(\mathbf{r}_c)$
Rh−Rh	0.015	−0.01	−0.01	+0.05	+0.03	0	0	0	+0.008	0.53	−0.008
	0.029	−0.02	−0.02	+0.08	+0.04	0	−0.003	−0.10	+0.013	0.45	−0.016
Rh−C_N	0.12	−0.14	−0.13	+0.66	+0.40	0.08	−0.04	−0.33	+0.14	1.17	−0.18
	0.12	−0.13	−0.13	+0.64	+0.39	0.01	−0.04	−0.33	+0.14	1.17	−0.18

[a] First line. [b] Second line. [c] $\nabla^2\rho_c$ = Laplacian of charge density at the BCP. λ_1, λ_2, λ_3 = eigenvalues of $\nabla^2\rho_c$ ($\nabla^2\rho_c = \lambda_1 + \lambda_2 + \lambda_3$). ϵ = bond ellipticity. $G(\mathbf{r}_c)$ = electronic kinetic energy density at the BCP. $V(\mathbf{r}_c)$ = electronic potential energy density at the BCP. $H(\mathbf{r}_c)$ = the total electronic energy density ($H(\mathbf{r}_c) = G(\mathbf{r}_c) + V(\mathbf{r}_c)$).

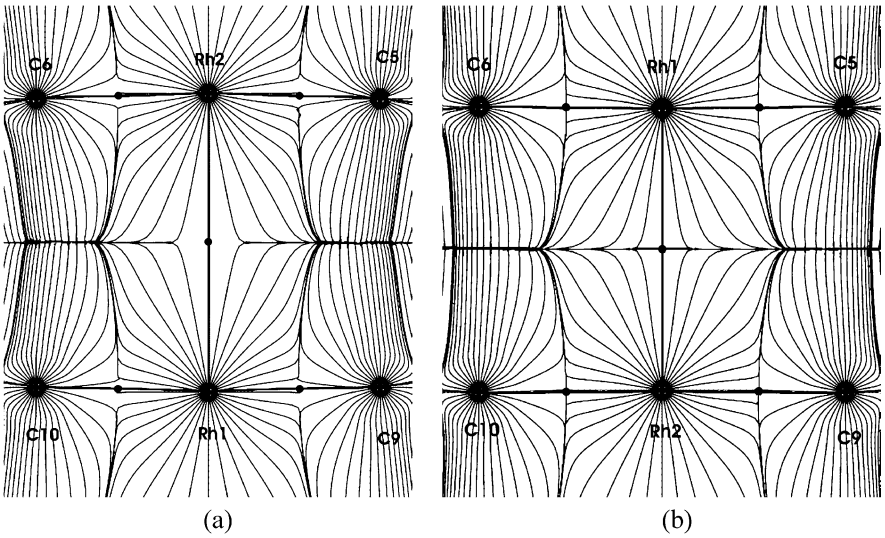

Figure 9. The trajectories of the gradient of the charge density in the plane defined by C9, C10, and Rh2 for the ground state (a) and excited triplet state (b) of eclipsed [Rh$_2$(diprop)$_4$]$^{2+}$. The bond paths are indicated by solid lines, and the bond critical points are denoted by filled circles. The graphs were generated with a locally modified version of TOPXD (Volkov, A.; Abramov, Y.; Coppens, P.; Gatti, C. *Acta Crystallogr., Sect. A* **2000**, *56*, 332−339).

triplet state, a bond path connects the two rhodium centers as shown in Figure 9. In both cases, the Laplacian is positive at the bond critical point (BCP),[26] as often observed for bonds involving metal atoms. It must be noted that in the case of bonds involving metal atoms the closed-shell versus open-shell classification based on the sign of $\nabla^2\rho_c$ at the bond critical point has been shown to be ambiguous, as it leads to the conclusion that all such bonds are of closed shell character, thus excluding any covalency.[29] A better description can be based on other properties such as the kinetic energy density $G(\mathbf{r}_c)$, the total electron energy density $H(\mathbf{r}_c)$, and the ratio of these quantities to $\rho(\mathbf{r}_c)$.

At the Rh−Rh BCP of the ground state, the kinetic energy density per electron $G(\mathbf{r}_c)/\rho(\mathbf{r}_c)$ is smaller than unity, while $V(\mathbf{r}_c)$ and $G(\mathbf{r}_c)$ have essentially equal values and, thus, $H(\mathbf{r}_c)$ is zero. In the excited state, the kinetic energy density at the BCP $G(\mathbf{r}_c)$ increases, but the negative value of $V(\mathbf{r}_c)$ decreases more, in agreement with the increase in the total charge density $\rho(\mathbf{r}_c)$ at the Rh−Rh BCP, leading to a more negative value of $H(\mathbf{r}_c)$ and $H(\mathbf{r}_c)/\rho(\mathbf{r}_c)$. Thus, the potential energy density $V(\mathbf{r}_c)$ dominates at the Rh−Rh BCP in the excited state indicating an increase in the open-shell character of the Rh−Rh interaction in the excited state. These

(29) (a) Koritsanszky, T. S.; Coppens, P. *Chem. Rev.* **2001**, *101*, 1583−1627. (b) Macchi, P.; Garlaschelli, L.; Martinengo, S.; Sironi, A. *J. Am. Chem. Soc.* **1999**, *121*, 10428−10429.

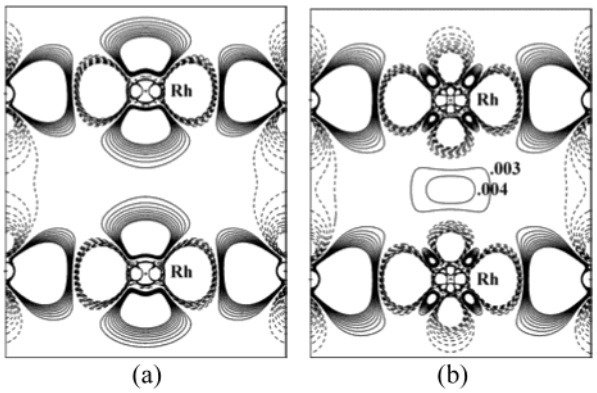

Figure 10. Theoretical deformation density maps of the ground state (a) and excited triplet state (b) of eclipsed $[Rh_2(diprop)_4]^{2+}$ in the plane of Rh1, Rh2, and carbon atoms. Contour levels are drawn at ±0.0015 au, and positive levels are solid lines, zero contour omitted.

observations are in agreement with the theoretical deformation electron density maps, which show that in the excited state there is an, albeit small, concentration of charge density in the Rh−Rh BCP region (Figure 10), similar to that observed for $[Pt_2(pop)_4]^{4-}$ ion.[10] No changes in the topological properties at the Rh−C_N bond critical points are observed upon excitation, in agreement with the very small changes of the Rh−C_N bond lengths in the excited state (Table 8).

The only pronounced difference for the twisted (Table S4) compared to the eclipsed geometry is found for the ground-state topological properties at the Rh−Rh BCP. The ground-state value of $H(\mathbf{r}_c)/\rho(\mathbf{r}_c)$ at the Rh−Rh BCP in the twisted geometry is >0, because of the dominance of $G(\mathbf{r}_c)$ over $V(\mathbf{r}_c)$, in agreement with longer Rh−Rh bond in the twisted structure.

In contrast to the AIM results, the analysis of the ELF of the ground state reveals no obvious bonding interaction between the rhodium atoms in both eclipsed and twisted geometries (Figure 11, $\eta(\mathbf{r}) = 0.77$). The Rh−C_N bonding region shows the localization domain close to the carbon atom, a feature previously described by Silvi et al.[30] as typical for dative bonds.

The ELF isosurface of the excited triplet state at $\eta(\mathbf{r}) = 0.77$ does not differ from that in the ground state for both eclipsed and twisted conformations and, thus, is not presented. However, at a lower ELF value $\eta(\mathbf{r}) = 0.24$, we observe a compact almost spherical in shape ELF domain located between the two metal atoms.[31] The formation of this ELF domain is consistent with the increase in Mayer bond order discussed above. The magnitude of the ELF value at which the metal−metal bonding is observed and the shape of the corresponding ELF domain resemble the ELF picture of Pt−Pt bonding in the $[Pt_2(pop)_4]^{4-}$ ion,[10] which similarly belongs to the family of d^8−d^8 complexes with paddle-wheel geometry. As in $[Pt_2(pop)_4]^{4-}$, we attribute the low value of the ELF for the Rh−Rh interaction to the small contribution of metal d-orbitals to the ELF.[32]

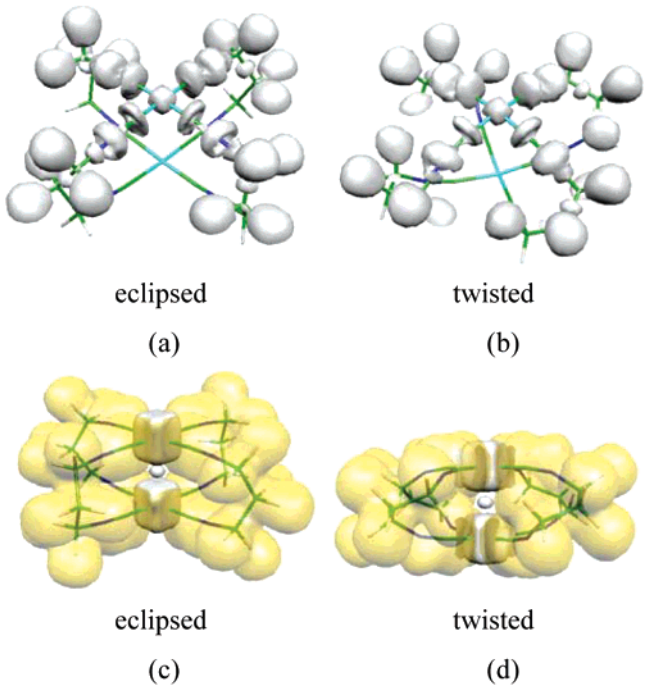

Figure 11. Electron localization function of $[Rh_2(diprop)_4]^{2+}$ in the eclipsed and twisted conformations on the ground-state (a, b) and excited-state (c, d) PES. In parts a and b, the plotted ELF value is 0.77; for clarity, only the ELF isosurface for the upper part of the molecule is shown. In parts c and d, the plotted ELF value is 0.24, and the localization domains of the two rhodium atoms and the Rh−Rh bonding region are colored in solid gray, while all other regions of ELF are shown in transparent yellow.

Conclusions

The DFT study of the $[Rh_2(diprop)_4]^{2+}$ ion reveals two energy minima on the ground-state and first excited-state potential energy surfaces corresponding to the eclipsed and twisted conformations, the eclipsed conformation being more stable by ~1 eV in both cases. The optimized geometry at the global energy minimum of the isolated $[Rh_2(diprop)_4]^{2+}$ ion is similar to that determined in the low-temperature X-ray single crystal study, though the Rh−Rh distances differ by 0.2 Å. The Rh−Rh distance in the eclipsed ground-state structure is shorter by 0.4 Å than that in the twisted conformation, in contrast to the trend observed in a series of structure determinations in which a shorter Rh−Rh bond corresponds to a larger twist angle. The difference may be attributed to the shortness of the diisocyano ligand which is distorted on twisting.

The excited-state potential energy surface similarly exhibits two minima corresponding to the eclipsed and twisted conformations. But in this case, the Rh−Rh distance is 3.1 Å in both geometries.

The results of the TD-DFT calculation of the singlet−singlet and singlet−triplet excitation energies are in reasonable agreement with the experimental observations. The lowest energy state is the singlet $^1A_2$ followed by the triplet state of interest $^3A_2$, corresponding to d_{z^2}*(metal antibonding) → p_z(ligand−metal bonding) transition.

The existence of Rh−Rh bond paths in the ground state and excited triplet state electron densities suggests weak

(30) (a) Krokidis, X.; Noury, S.; Silvi, B. J. *Phys. Chem. A* **1997**, *101*, 7277−7282. (b) Pilme, J.; Silvi, B.; Alikhani, M. E. *J. Phys. Chem. A* **2003**, *107*, 4506−4514.

(31) Llusar, R.; Beltran, A.; Andrés, J.; Fuster, F.; Silvi, B. *J. Phys. Chem. A* **2001**, *105*, 9460−9466.

(32) Kohout, M.; Savin, A. *J. Comput. Chem.* **1997**, *18*, 1431−1439.

bonding metal−metal interaction in both states. However for the ground state, this observation is not supported by the electron localization function (ELF). In contrast to the ground state, the excited-state ELF at low values exhibits a low maximum in the Rh−Rh region, indicating Rh−Rh weak covalent bonding upon excitation of the complex, in agreement with the calculated Mayer Rh−Rh bond order which increases from a very low value to close to unity on excitation.

Acknowledgment. Financial support of this work by the National Science Foundation (CHE0236317) and the Petroleum Research Fund of the American Chemical Society (PRF37614AC3) is gratefully acknowledged. The computations were performed on the 64-processor SGI Origin3800, 32-processor Sun Blade 1000 (UltraSparc III) and 48-processor Sun Ultra-5 (UltraSparc IIi) supercomputers at the Center for Computational Research of the State University of New York at Buffalo which is supported by a grant (DBI9871132) from the National Science Foundation.

Supporting Information Available: Tables of the atomic-orbital contributions to the frontier molecular orbitals (in %) and Mulliken spin populations for both eclipsed and twisted geometries. Tables of the difference in the population of the valence atomic orbitals and topological properties at the Rh−Rh and Rh−C_N BCPs for the twisted geometry. Listing of Cartesian coordinates of the four optimized geometries. This material is available free of charge via the Internet at http://pubs.acs.org.

IC035243H